

## Numerical study of the Kondo cloud using finite-U slave bosons

L. C. Ribeiro

Centro Federal de Educação Tecnológica Celso Suckow da Fonseca CEFET/RJ, Campus Nova Iguaçu, 26041-271, Nova Iguaçu-RJ, Brazil

G. B. Martins\*

Instituto de Física, Universidade Federal Fluminense, 24210-346 Niterói, RJ, Brazil

G. Gómez-Silva and E. V. Anda

Departamento de Física, Pontifícia Universidade Católica do Rio de Janeiro (PUC-Rio), RJ, 22453-900, Brazil



(Received 25 March 2018; revised manuscript received 14 February 2019; published 26 February 2019)

In this work, using the finite-U slave boson mean-field approximation to solve the single-impurity Anderson model, the authors apply two different strategies to study the Kondo cloud, by analyzing quantities that are dependent on the distance to the magnetic impurity and then finding a universal distance scale  $\xi_K$  through the collapse of the results into an universal function. The first method is based on the analysis of the local density of states of the conduction electrons (denoted as  $\xi_K^L$ ), while the second relies on the analysis of spin correlations ( $\xi_K^S$ ). Our calculations show that there is exact quantitative agreement, in the way  $\xi_K$  depends on  $U/\Gamma$ , between  $\xi_K^S$  and the results obtained through the heuristic expression  $\xi_K \propto v_F/\Gamma_K$ , while there is very close quantitative agreement between  $\xi_K^S$  and  $\xi_K^L$ . The use of the slave boson technique to calculate the spin correlations, which eliminates finite size effects, allowed us to study very large Kondo clouds, something that is very difficult using other techniques, like the density matrix renormalization Group method, for example. In addition, the very smooth curves obtained for the spin correlations allowed us to qualitatively identify a region in the Kondo cloud, adjacent to the impurity, that had been connected to the free orbital fixed point in previous numerical renormalization group calculations [Phys. Rev. B **84**, 115120 (2011)].

DOI: [10.1103/PhysRevB.99.085139](https://doi.org/10.1103/PhysRevB.99.085139)

### I. INTRODUCTION

Since the measurement of the Kondo effect [1,2] in quantum dots (QDs) by the group of Mark Kastner in 1998 [3], there has been a revival of interest in proposals for experimentally observing the so-called Kondo “cloud,” which occupies a mesoscopically sized region containing the spin density of conduction electrons screening a localized magnetic moment that is coupled to a Fermi sea. The extension of this cloud is associated to the Kondo length scale  $\xi_K$ . In more formal terms, in the same way that the Kondo temperature  $T_K$  represents a universal energy scale for the Kondo state, renormalization arguments suggest that, deep in the Kondo regime, physical observables measured at a distance  $r$  from the localized magnetic moment should vary as  $r/\xi_K$ . While the physics associated to the Kondo temperature  $T_K$  is well known, that associated to  $\xi_K$  (and the Kondo cloud) is more controversial [4]. An heuristic estimation of  $\xi_K$  takes in account that conduction electrons scattered off the Kondo resonance, which has width  $k_B T_K$ , traveling with the Fermi velocity  $v_F$ , will have a lifetime  $\sim \hbar/k_B T_K$ . Thus the Kondo length scale can be estimated as  $\xi_K = \hbar v_F/k_B T_K$ , where  $k_B$  and  $\hbar$  are the Boltzmann and Planck constants, respectively. For  $T_K = 1$  K and typical Fermi velocities,  $\xi_K$  ranges between 0.1 to 10  $\mu\text{m}$ . As discussed below, the experimental observation of a Kondo length scale in this

range of values has a long and mostly unsuccessful history, leading to controversies regarding its actual existence. One often cited puzzle [5], for example, is that systems with Kondo clouds much larger than the interimpurity separation have properties, like magnetic susceptibility and resistivity, that are *linear* in magnetic impurity concentration and well-described theoretically by *single-impurity* models.

In this paper, we considerably improve on a previous theoretical proposal, made by some of the authors, to numerically evaluate  $\xi_K$  using the local density of states (LDOS) [6]. We also compare our new results for  $\xi_K$  with those obtained by using spin correlations. More specifically, we study a one-dimensional (1d) system, consisting of a magnetic moment coupled to a 1d metallic chain, and use the LDOS in the chain sites to probe the Kondo cloud. The details will be described in Sec. III and an schematic description of the method is shown in Fig. 1. As extensively argued below, recent experimental developments in unrelated fields (adsorbates in metallic surfaces [7], cold atoms [8,9], circuit-QED [10], etc.) raise the possibility of directly building, in the laboratory, systems akin to the one proposed here, which was once considered as just a toy model. Thus, to substantiate our choices of a 1d system and of the LDOS as one of the possible physical quantities to be measured, in the next sections, we review the literature for spin- and LDOS-based experimental attempts to measure  $\xi_K$ , as well as theoretical proposals to detect the Kondo cloud. Given that the detection of the Kondo cloud continues to be an

\*Corresponding author: gbmartins@ufu.br

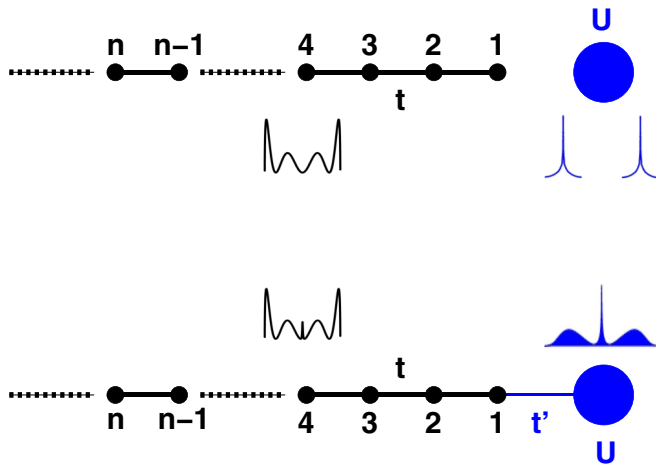


FIG. 1. Anderson impurity, with Coulomb interaction  $U$ , coupled by a hopping  $t'$  to a semi-infinite tight-binding chain with half-bandwidth  $D = 2t$ . Top panel illustrates the situation when there is no Kondo effect ( $t' = 0$ ). The black curve under the chain is the LDOS of site  $n = 4$ . Bottom panel illustrates the situation when the Kondo state is formed (finite  $t'$ ). Notice the change in the LDOS of site  $n = 4$ , mainly around the Fermi energy, when comparing upper and lower panel.

open problem, we will see that there have been many recent theoretical proposals to accomplish its detection. Some of them include using cold atoms, quantum entanglement ideas probed in the orbital Kondo effect in a double QD system, QED circuits, etc. We obviously do not try to exhaust this extensive field of research, as the idea here is just to place our proposal in the context of what can be experimentally done, and which proposals have been already made.

### A. Using spin to measure the Kondo cloud: NMR

Attempts to observe the Kondo cloud have a reasonably long history. Although the initial fingerprint of the Kondo effect was obtained through resistivity measurements in gold and silver samples in 1936 [11], once Jun Kondo recognized in the early 1960s [1] that the effect was eminently connected to the exchange interaction of conduction electrons with *isolated* magnetic impurities, it did not take long for nuclear magnetic resonance (NMR) to be used for probing the Kondo cloud. A quarter of a century before the QD breakthrough, Boyce and Slichter [12,13] used Knight shift measurements (an NMR technique to measure Pauli paramagnetism) to detect the Kondo cloud in samples of copper with diluted Fe impurities (CuFe alloys) [14]. The Knight shift can measure the local susceptibility  $\chi(r)$  of the conduction electrons at subsequent shells of Cu atoms around a Fe magnetic impurity. The expectation was that once the temperature was lowered below the Kondo temperature  $T_K$ , and the Kondo state was formed, the conduction electron polarization present in the Kondo cloud would shift the NMR line of the Cu nuclei (the Knight shift) close to an Fe impurity. Unfortunately, no shift was observed, aside from that coming from the Pauli susceptibility. It turns out (see Ref. [4]) that the local susceptibility  $\chi(r)$ , measured by NMR ( $r$  is the distance from the impurity), factors into

the product of two  $r$ -dependent functions: (i) the first one, which signals the presence of the Kondo cloud, varies too slowly with  $r$  to be picked up by the NMR signal, and (ii) the second one, which varies as  $r^{-3}$ , makes  $\chi(r)$  vanish before an oscillation caused by the Kondo part could be detected. This discussion indicates that measurements involving spin seem to suffer from very stringent limitations. Given the large size of the Kondo cloud, and the fact that it is comprised by a single compensating spin, one may argue that the spin density in the Kondo cloud is spread so thinly that it resembles more a Kondo “fog” [15]. One additional factor may contribute to complicate the situation: the spin screening is not static, it is a dynamic spin-flip process (quantum fluctuations) that would require measurements at frequencies around tens of gigahertz [16].

### B. Using the LDOS to measure the Kondo cloud: STM

The spin flipping process just mentioned can be qualitatively described as the result of the impurity electron, located at a level  $\epsilon_d$  below the Fermi energy  $\epsilon_F$ , being virtually excited to the Fermi surface. The reverse process will bring an electron with *opposite* spin from  $\epsilon_F$  to  $\epsilon_d$ . A coherent sequence of these processes establishes a spin-singlet state between the impurity electron and a delocalized conduction electron, forming the Kondo cloud. In addition, the frequent “visits” of the impurity electron to the Fermi surface causes its LDOS to acquire spectral weight at  $\epsilon_F$ , the so-called Abrikosov-Suhl resonance (or Kondo peak), with a width  $k_B T_K$ . However, in addition to that, the LDOS of the conduction electrons is also altered at the Fermi energy. This reflects the LDOS counterpart to the  $r$ -dependent spin polarization in the Kondo cloud, which NMR failed to measure. This Kondo peak “echo” in the LDOS of the Fermi sea is evident in lattice models, especially in 1d, as is our case, where an alternating sequence of resonances and antiresonances at  $\epsilon_F$ , in the chain sites, can be seen as one moves away from the impurity, as schematically shown in Fig. 1 (for additional details, see our previous work, Ref. [6]). This behavior resembles the Kondo-mirage effect seen in quantum corals [17]. Therefore, it seems only natural, rather than using spin polarization to probe the Kondo cloud, to look into variations in the LDOS  $\rho(\vec{r})$  at a distance  $\vec{r}$  from the impurity.

Incidentally, in the same year as the QD breakthrough [3], using a scanning tunneling microscope (STM) to measure differential conductance  $dI/dV$ , two groups independently reported the observation of the Kondo effect occurring in Cerium adatoms on Ag(111) surfaces [18] and Cobalt adatoms on Au(111) surfaces [19]. As  $dI/dV \propto \rho(\vec{r})$ , these STM results could potentially observe the Kondo cloud. Since then, many measurements to observe the Kondo effect in magnetic impurities adsorbed on metallic surfaces have been performed using STM [7,17,20–32]. For a review of STM experiments involving Kondo in adatoms up to 2009, see M. Ternes *et al.*, Ref. [33]. These initial measurements [18,19] were shortly thereafter partially reproduced by a conduction electron LDOS calculation through a combination of first principles band structure and many-body [noncrossing approximation (NCA)] calculations [34]. The main discrepancy

between measurements and theory, as described in more detail below, were that the measured STM signal vanished a short distance from the impurity ( $\approx 10 \text{ \AA}$ ), while theory predicted a long-range signal with a periodic oscillation of the shape of the resonance.

Being a local probe with high space- and energy-resolution, STM seemed particularly well suited for observing the Kondo cloud. In that respect, the theoretical predictions of Újsághy *et al.* [34] (see also Refs. [35,36]) indicated that the Kondo resonance on an adsorbed magnetic impurity induces strong spectroscopic signatures in the conduction electron LDOS around the Fermi energy, with line shapes that oscillate between asymmetric Fano and Lorentzian with distance to the impurity. The theory reproduced the Fano line-shape observed when the STM tip was located right above the impurity, but the measurements did not show the extended range of the signal nor the line-shape oscillation. For example, Madhavam *et al.* [19] (see also N. Knorr *et al.*, Ref. [21]) reported that the asymmetric Fano line-shape, observed when the STM tip is located above a Co atom in Au(111), turned into a flat signal  $\approx 10 \text{ \AA}$  away from the impurity, with a continuous loss of asymmetry in the line-shape up to  $\approx 4 \text{ \AA}$ . Note that the asymmetry in the line shape was initially explained as an interference effect, as studied previously by Fano for similar noninteracting systems [37], although this effect was later recognized as not being actually responsible for the Fano line-shape [34,38]. It should also be noted that, calculations by Schiller and Hershfield [35], using NCA to calculate the impurity's dressed Green's function and a tight-binding model to calculate the surface's Green's function, produced results in agreement with the limited spatial extent of the Kondo resonance obtained in the experiments. An important point to consider is what conduction electron states (bulk and/or surface) couple more strongly to the adatom [38]. Experimental evidence [21] seems to indicate that bulk states couple much more strongly to the impurity than surface states.

It was then a surprise when Prüser *et al.* [30,31] reported the observation of a *long-range* Kondo signature for single magnetic atoms of Fe and Co *buried* a few layers under a Cu(100) surface. Their experimental results, supported by self-consistent calculations, showed a periodic variation in line shape away from the impurity, as well as the persistence of a Kondo-like signal much farther away from the impurity than in previous results. These measurements, and their interpretation, relied on an effect called “electron focusing” [39]: specific anisotropies of a metal's Fermi surface result in strong directional propagation of quasiparticles, which, after scattering off the buried magnetic impurity, are detected by the STM tip at the surface of the metal. Their modeling of the results showed that the line-shape characterizing the STM Kondo signal is directly connected to the band structure of the host crystal, making clear that the initial interference explanation of the Fano line shape is too simplistic. One should also note that a realistic calculation by Dang *et al.* for Co and Mn adsorbed into a Cu(111) surface, see Ref. [40], using a combination of density functional theory (Korringa-Kohn-Rostoker method) and two different impurity solvers (continuous time quantum Monte Carlo and exact diagonalization), covering a range of temperatures and different impurity fillings, and, more importantly, taking all five 3d

orbitals in account, showed a quite intricate combination of effects leading to a complex variation of the expected STM spectra with distance from the impurity. In conclusion, using the STM of transition metal ions adsorbed in metallic surfaces (or buried under them) as a route to study the Kondo cloud is a promising avenue. However, as just described, this route seems to involve too many additional aspects (like multiorbital Kondo, dependence with filling and double counting of correlations [40]; which state—surface or bulk—couples more strongly to the adsorbate [38]; buried versus adsorbed [30], etc.) to unmistakably characterize experimentally the Kondo cloud.

However, despite the complications just mentioned, given that STM *did observe* long-range signals [30,31], one would still like to use the probing of changes in  $\rho(\vec{r})$  to detect the Kondo cloud, but maybe in a simpler environment, for example, a linear chain, like the one recently used by N. Néel *et al.* [7] to study the competition between Kondo and RKKY for two Cobalt atoms attached at the ends of a short Copper chain.

Other examples of one-dimensional mesoscopic systems that could be used to probe the properties of the Kondo cloud, include, for example, a very interesting proposal [10] involving a one-dimensional circuit-QED setup consisting of a Cooper pair box coupled to a chain of Josephson junctions. The authors of this work find that there is a deep connection of the ground state of this system with that of the Kondo state. They also point out that their results for this circuit-QED system point to the universality of its ground state, as in the Kondo state. Along the line of “Kondo-box” ideas [41], a few proposals [42–44] involve connecting a QD to 1d wires of finite length  $L$ . Since the conductance  $G$  through the QD is a probe of the Kondo state, an experimental study of  $G(L)$  would provide information on  $\xi_K$ . A variation of the Kondo-box idea was proposed by J. Park *et al.* in Ref. [45]. In that work, in a system involving a QD connected to metallic leads, a kind of Kondo box is created by applying a gate voltage beyond a distance  $L$  from the QD. Poor-man's scaling, numerical renormalization group (NRG), and Fermi liquid theory are used to study the change in the properties of the system (mostly conductance  $G$  and  $T_K$ ) with  $L$  to detect the Kondo cloud and estimate  $\xi_K$ . It should be noted that it is not really a *physical* Kondo box that is being proposed, but rather a systematic perturbation of the electron states at the edges of the Kondo cloud, by varying the orbital energy of conduction electrons on sites located a distance  $r \geq L$ .

Another example of 1-dimensional system to probe the Kondo cloud involves the metallic edge states in two-dimensional (2d) topological insulators. The theoretical prediction of the existence of the quantum spin Hall state [46] and its observation in HgTe quantum wells [47] (see Ref. [48] for a detailed review) has spurred a wave of new research involving the metallic helical states circling the edge of a 2d topological insulator. An interesting work [49,50] studies the coupling of a magnetic moment (in an antidot) with these helical states (which act as contacts) and concludes that the measurement of the space- and time-resolved current cross correlations can directly detect the Kondo cloud and even resolve it spatially.

In addition, we mention two theory papers that describe cold atom systems whose ground states are of the Kondo type.

In the first, Y. Nishida [8] proposes a cold atom set up that exhibits an SU(3) orbital Kondo state. Shortly thereafter, J. Bauer *et al.* [9] proposed a mixture of  $^{40}\text{K}$  and  $^{23}\text{Na}$  atoms whose low-energy physics they describe with an Anderson impurity model (AIM). According to the authors, current atomic physics spectroscopic tools could be applied to measure the equal time spin correlation function away from the impurity, providing a finger print of the Kondo cloud. These systems could, in principle, be built in a one-dimensional optical lattice.

As already mentioned above, in the last few years, given that the Kondo cloud detection is still an open problem, alternative ways of theoretically analyzing it have been developed. Notable among new theoretical tools are the ones that rely on entanglement ideas. With the development of nanostructures capable of performing, at least in a limited scale, quantum computations and manipulating quantum information, concepts like entanglement entropy in condensed matter systems gained in popularity (see Ref. [51] for a comprehensive review, especially Sec. 4.2, about the Kondo state). Using a variational ground state introduced by Yosida [52], S. Oh and J. Kim [53] presented results analyzing the entanglement of the quantum impurity to the conduction electrons. These results were followed by a series of works by Affleck and collaborators [54–56] where the structure of the Kondo cloud was specifically addressed using entanglement concepts. To that end, an especially interesting result is presented in Ref. [57], where it is shown through numerical calculations that an impurity coupled to the end of a spin chain with nearest and next-nearest antiferromagnetic couplings (a  $J_1$ - $J_2$  spin chain, or, an open frustrated Heisenberg chain), in a certain regime of parameters (when  $J_2$  is equal to a critical value above which the spin chain becomes dimerized, i.e., the spectrum becomes gapped), has low-energy long distance physics equal to that of the Kondo model (note that H. Frahm and A. Zvyagin had noted this connection to the Kondo problem as early as 1997 [58]). This impurity- $J_1$ - $J_2$  model was then used to do extensive entanglement studies of the Kondo cloud by Affleck’s group [54–56]. One interesting result was the heuristic description of  $\xi_K$  as the length of the “impurity valence bond” (IVB). Indeed, one can use a “resonating valence bond” basis (essentially singlets connecting two spins in the chain) to describe the ground state of a spin chain; for an even number of sites the impurity will always be part of a valence bond, the IVB. One may argue that the typical length of this IVB can be associated to  $\xi_K$  (see Ref. [56] and references therein for details).

The Kondo physics in the impurity- $J_1$ - $J_2$  model was analyzed by other groups to study the Kondo cloud by using different definitions of entanglement entropy. For example, A. Bayat *et al.* [59] used the so-called negativity to measure entanglement and with it determine  $\xi_K$  and found that the impurity spin is indeed maximally entangled with the Kondo cloud. The same group uses again the same spin chain model to study the role of the Kondo cloud in quench dynamics [60] and also on the RKKY interaction between two impurities placed on the  $J_1$ - $J_2$  spin chain [61]. More recent approaches have used specialized tools of quantum information, like “entanglement of formation” and “entanglement witness operators” [62], as well as “concurrence” [63] to study the Kondo state. For

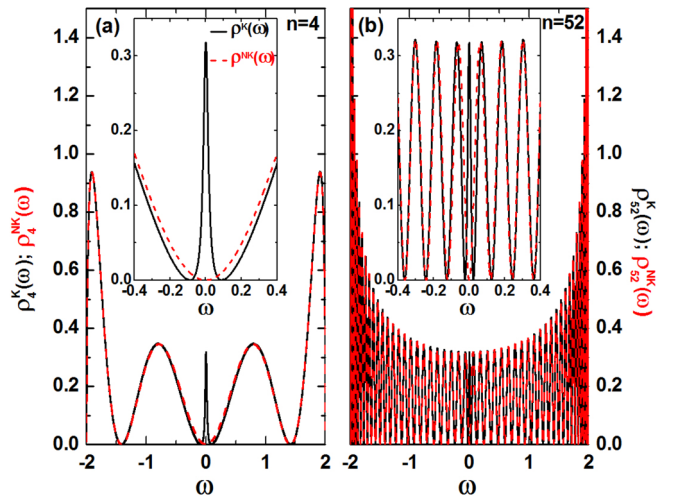


FIG. 2. LDOS at sites  $n = 4$  and  $52$  inside the tight-binding chain, in (a) and (b), respectively. Results are shown when the impurity is coupled to the chain, for  $U = 1.25$  and  $U/\Gamma = 10.0$  [(black) solid line], and when it is decoupled from it [ $\Gamma = 0.0$ , (red) dashed line]. The inset in each panel shows a zoom of the main-panel data around the Fermi energy. A finite  $\Gamma$  results in a Kondo state, while a vanishing  $\Gamma$  suppresses it, and the difference between the two corresponding LDOS is used to calculate the Kondo cloud extension function  $L(n)$  [see Eq. (7)].

example, C. Yang and A. Feiguin [63] have proposed the use of concurrence, which measures entanglement, to analyze the properties of the Kondo cloud. In addition, they have used the idea of “projected natural orbitals” to study the Kondo state and contrast its properties at the weak and strong coupling regimes. Similar ideas have been also applied through the use of the so-called Natural orbitals renormalization group approach [64] to study the properties of a “natural orbital” single conduction electron state that is involved in screening more than 90% of the impurity spin. Finally, G. Yoo *et al.* [65], studying single and double quantum dot systems, were able to directly relate the entanglement entropy (between the impurity spin and the conduction electrons) with the total conductance through a double QD system setup in the orbital Kondo regime, which could then be manipulated by electrical gates, uncovering the spatial properties of the Kondo cloud.

An important parentheses should be opened here: as presented in our previous work (Ref. [6]), as well as in the present manuscript, and related publications from other groups (see, for example, Ref. [66]), the observation by STM of *some* Kondo-peak-related effect in the LDOS at sites away from the impurity (see, for example, the insets in both panels of Fig. 2) can be considered as a trivial effect that, by itself, is not able to uncover the *spatial* scaling properties of the Kondo cloud. For that, it is necessary to measure this effect in each site for all values of energy, integrate them, subtract the effects in the absence of the impurity [see Eqs. (6) and (7)] and then analyze the spatial dependence of the obtained results. Noise and measurement errors should make it all but impossible to obtain STM results that allow for a scaling analysis, unfortunately. That is not to say the results to be described in this work are worthless. There are systems (already mentioned

above [10]) whose low-energy physics can be described by the dissipative two-level model (DTLM), which can then be mapped to the anisotropic Kondo model (AKM) [67]. That is the case, for example, of a Cooper-pair-box coupled to a chain of Josephson junctions, a so-called circuit-QED setup, as described in Ref. [10]. In that work, the authors analyzed the equivalent to the Kondo cloud spin correlations (see Eq. (7) in Ref. [10]) and proposed a way of measuring it with a “comb” of local gates applied along the chain of Josephson junctions. Here, we speculate that one can do a “reverse mapping” (from the AKM back to the DTLM) and find what quantity is equivalent to the AKM chain-site LDOS. This may offer the possibility of performing spatial scaling measurements of the Kondo cloud of the LDOS-type described next.

In this work, we present two methods to study the Kondo screening cloud in a system composed by a single magnetic impurity, with Coulomb interaction  $U$ , coupled to a charge reservoir (see bottom panel in Fig. 1). The charge reservoir will be modeled by a semi-infinite chain, therefore the results obtained here describe either a QD embedded between metallic leads or a Cobalt ion, for example, coupled to a Copper chain adsorbed onto a metallic surface, a system that can be experimentally probed by STM [7]. The first method uses the LDOS along the semi-infinite chain to characterize the Kondo cloud, and therefore could be tested, in principle, by STM. The second method is based on probing spin-spin correlations, as done along the years (for both the Kondo and the Anderson models) by several groups, using different techniques (details can be found in Refs. [16,68–71]). We will show that our method to obtain the spin correlations, based on the finite-U slave boson mean-field approximation (SBMFA) [72], has a few advantages when compared to other methods, like DMRG [70,71], for example. As mentioned above, the Kondo screening length can be estimated through the equation

$$\xi_K^{v_F/T_K} = \hbar v_F / k_B T_K, \quad (1)$$

where  $v_F$  is the Fermi velocity of the electrons in the charge reservoir. As has been done in previous studies of the Kondo screening length (see, for example, Refs. [70,71]), we compare the results obtained by our two different methods to the ones obtained using Eq. (1), where we use the value of  $T_K$  as obtained by the finite-U SBMFA.

As will be shown below, an interesting outcome of our results was the identification of a region adjacent to the impurity where the universality of the  $r$ -dependent quantities we probed (LDOS and spin correlations) was lost (where  $r$  measures the distance to the impurity). This loss of universality was qualitatively associated to NRG results presented in Ref. [66], where this region was connected to the free orbital fixed point (see discussion around Fig. 6). The identification of what could be called an internal structure of the Kondo cloud, and how it varies with the single impurity Anderson model (SIAM) parameters, could be a further step into providing ways of experimentally detecting this very elusive many-body quantum state.

The rest of the paper is organized as follows. In Sec. II, we present the details of the Hamiltonian for the SIAM. This is followed by Sec. III, where the LDOS-based method is presented, together with the numerical results obtained

through it for the Kondo cloud extension (see Fig. 4), denoted as  $\xi_K^L$ . Then, Sec. IV introduces the spin correlations method and the corresponding results obtained for the cloud extension (see Fig. 5), denoted as  $\xi_K^\Sigma$ . Section V compares the results obtained through both methods to those obtained by using Eq. (1), in addition to a summary of the main results, as well as our conclusions. Finally, in Appendix, we present details of the finite-U SBMFA.

## II. SINGLE-IMPURITY ANDERSON MODEL HAMILTONIAN

The total Hamiltonian has the following terms:

$$H_T = H_{\text{imp}} + H_{\text{band}} + H_{\text{hybrid}}, \quad (2)$$

where  $H_{\text{imp}}$  and  $H_{\text{band}}$  represent the Hamiltonian of the impurity and the noninteracting band, respectively, and  $H_{\text{hybrid}}$  is the hybridization between them:

$$H_{\text{imp}} = V_g \sum_{\sigma} n_{d\sigma} + U/2 \sum_{\sigma} n_{d\sigma} n_{d\bar{\sigma}}, \quad (3)$$

$$H_{\text{band}} = t \sum_{n=1, \sigma}^{\infty} (c_{n\sigma}^{\dagger} c_{n+1\sigma} + c_{n+1\sigma}^{\dagger} c_{n\sigma}), \quad (4)$$

$$H_{\text{hybrid}} = t' \sum_{\sigma} (c_{d\sigma}^{\dagger} c_{1\sigma} + c_{1\sigma}^{\dagger} c_{d\sigma}), \quad (5)$$

where  $c_{d\sigma}^{\dagger}$  creates an electron with spin  $\sigma = \uparrow, \downarrow$  at the impurity,  $n_{d\sigma} = c_{d\sigma}^{\dagger} c_{d\sigma}$  is the number operator at the impurity, and  $c_{n\sigma}^{\dagger}$  creates an electron with spin  $\sigma$  at the  $n$ th site of the semi-infinite chain. The gate potential  $V_g$  controls the position of the localized level of the impurity in relation to the Fermi energy  $\epsilon_F = 0$  of the band, while the Coulomb repulsion between two electrons occupying the impurity's localized level is given by  $U$ . The broadening of the impurity level is given by  $\Gamma = 2\pi t'^2 \rho_{\text{band}}(\epsilon_F)$ , where  $\rho_{\text{band}}(\epsilon_F)$  is the LDOS of the first site in the semi-infinite chain at the Fermi energy  $\epsilon_F$  and  $t'$  is the hopping between the impurity and the first site of the semi-infinite chain. Our unit of energy is the hopping in the semi-infinite chain, denoted  $t$  (see Fig. 1), therefore the half-bandwidth is  $D = 2.0$ . We will analyze how  $\xi_K$  varies for different values of  $\Gamma$ , keeping  $U = 1.25$ , unless stated otherwise. All calculations were done at the particle-hole symmetric point  $V_g = -U/2$ .

## III. KONDO CLOUD EXTENSION OBTAINED THROUGH LDOS

In two previous works by some of the authors (see Refs. [6,73]), it was proposed a strategy to probe the Kondo cloud extension  $\xi_K$  that relied on measuring the *distortion* caused by the Kondo resonance (which occurs *at* the impurity) in the LDOS of sites in the Fermi sea. Figures 1 and 2 explain how that is accomplished. The top panel in Fig. 1 illustrates the situation when the impurity (in blue, on the right side) is disconnected from the charge reservoir ( $t' = 0$ ) and therefore the Kondo state does not form [74]. The black curve right below the chain shows  $\rho_{n=4}^{\text{NK}}(\omega)$ , i.e., the LDOS of site  $n = 4$  in the absence of the Kondo state (“NK” stands for non-Kondo). The (red) dashed curve in the main panel in Fig. 2(a) shows

the details of  $\rho_{n=4}^{\text{NK}}(\omega)$ , with a zoom around the Fermi energy shown in the inset. On the other hand, in the bottom panel of Fig. 1, we reconnect the magnetic impurity to the semi-infinite chain (finite  $t'$ ), allowing for the formation of a Kondo state. Notice the presence of the Kondo peak at the Fermi energy on the impurity's LDOS [(blue) gray shaded curve above the impurity in the bottom panel]. The crucial point displayed in this figure is that the Kondo peak at the impurity induces a corresponding peak (at the Fermi energy) in the LDOS of the  $n = 4$  site, which is schematically shown by the black curve above the lower panel chain (denoted  $\rho_{n=4}^{\text{K}}(\omega)$ , where “K” stands for Kondo). Again, the details of  $\rho_{n=4}^{\text{K}}(\omega)$  are displayed by the black solid curve in Fig. 2(a). Figure 2(b) shows that the peak at the Fermi energy in  $\rho_n^{\text{K}}(\omega)$  is still present for site  $n = 52$ , although it is now narrower than the one in panel (a) for  $n = 4$ . Note that the procedure to calculate the LDOS inside the chain in the Kondo state has been described in detail in Ref. [6], here we will provide just a brief outline of it: after calculating the dressed Green's function at the impurity site (in this paper, we use the finite-U SBMFA for that), we use an equation of motion (EOM) method to calculate the Green's function at an arbitrary site  $n$  inside the chain, and from it we obtain the LDOS  $\rho_n^{\text{K}}(\omega)$  [75]. On the other hand,  $\rho_n^{\text{NK}}(\omega)$  can be obtained exactly as it requires the solution of an independent electron problem. A very similar idea, based in the use of the EOM, was used in Ref. [66] to study the properties of the Kondo cloud using NRG. In that work, the authors define regions *inside* the Kondo cloud that are clearly associated to the fixed points occurring in the RG flow of the SIAM and which seem to unveil an internal structure of the Kondo cloud. Our results indicate the possibility that we are seeing signals of this structure in the region close to the impurity.

We now describe how we can use  $\rho_n^{\text{K}}(\omega)$  and  $\rho_n^{\text{NK}}(\omega)$  to obtain  $\xi_K$ . Intuitively, one can loosely say that the difference between these two LDOS, after integrating in energy, should contain a snapshot of the Kondo cloud at site  $n$ . Obviously, an integral in energy of  $\rho_n^{\text{K}}(\omega) - \rho_n^{\text{NK}}(\omega)$  over  $-\infty \leq \omega \leq \infty$  vanishes, therefore a different strategy should be adopted. In our previous work [6], the distortion caused by the Kondo state was quantified by the absolute value of the function  $F(n)$ , as defined by

$$F(n) = \int_{-\infty}^{\infty} [\rho_n^{\text{K}}(\omega) - \rho_n^{\text{NK}}(\omega)] L_{\Delta}(\omega) d\omega, \quad (6)$$

where  $L_{\Delta}(\omega)$  is a Lorentzian distribution with a width  $\Delta$  that is controlled by the Kondo temperature. This strategy provided results for  $\xi_K$  that were in agreement with other methods (see Ref. [6] for details).

In the present work, we will make a modification to the definition of  $F(n)$  [and rename it  $L(n)$ ], by removing the convolution with the Lorentzian and taking instead the absolute value of the difference  $\rho_n^{\text{K}}(\omega) - \rho_n^{\text{NK}}(\omega)$ , namely,

$$L(n) = \int_{-\infty}^{\infty} |\rho_n^{\text{K}}(\omega) - \rho_n^{\text{NK}}(\omega)| d\omega. \quad (7)$$

The main motivation to make this modification [76] is as follows. As emphasized by Anderson through his poor-man's scaling analysis of the Kondo effect, using a perturbative

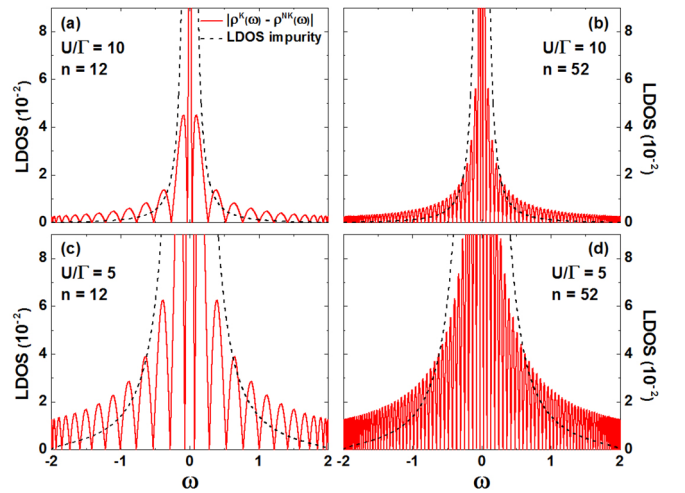


FIG. 3. The (red) solid curves show  $|\rho_n^{\text{K}}(\omega) - \rho_n^{\text{NK}}(\omega)|$  results for  $U/\Gamma = 10.0$  [(a) and (b)] and  $U/\Gamma = 5.0$  [(c) and (d)] at sites  $n = 12$  [(a) and (c)] and  $n = 52$  [(b) and (d)]. The black dashed curves are the LDOS at the impurity (the Kondo peak), equivalent to the  $L_{\Delta}(\omega)$  used in our previous method [6] [see Eq. (6)]. It is clear that a convolution with  $L_{\Delta}(\omega)$  suppresses spectral weight at higher energies. In addition, by comparing the left-side panels with the right-side panels it is easy to see that, for fixed  $\Gamma$ , the envelope function of  $|\rho_n^{\text{K}}(\omega) - \rho_n^{\text{NK}}(\omega)|$  depends very weakly on  $n$ . All results obtained for  $U = 1.25$ .

renormalization group approach [77], all energy scales (up to a cutoff given by  $D$ , the half-bandwidth) contribute to the Kondo state. The consequence of that in our calculation can be appreciated in Fig. 3, where  $|\rho_n^{\text{K}}(\omega) - \rho_n^{\text{NK}}(\omega)|$  results are shown for  $n = 12$  (left-side panels) and 52 (right-side panels), for  $U/\Gamma = 10.0$  (top panels) and 5.0 (bottom panels), for  $U = 1.25$ . A Lorentzian  $L_{\Delta}(\omega)$  (black dashed curve) centered around the Fermi energy, and with a width given by the associated Kondo temperature, is also shown, highlighting that although its convolution with  $\rho_n^{\text{K}}(\omega) - \rho_n^{\text{NK}}(\omega)$  [as done in our previous method, see Eq. (6)] preserves the LDOS difference around the Fermi energy, it suppresses it at higher energies. Thus the convolution done with  $L_{\Delta}(\omega)$ , besides artificially introducing  $T_K$  into the calculation of  $\xi_K$ , was also suppressing higher energy contributions to it.

In addition, it is also interesting to remark that a comparison between the left- and right-side panels in Fig. 3 indicates that  $|\rho_n^{\text{K}}(\omega) - \rho_n^{\text{NK}}(\omega)|$  presents an envelope function which is very weakly dependent on  $n$ . As the number of oscillations in  $|\rho_n^{\text{K}}(\omega) - \rho_n^{\text{NK}}(\omega)|$  increases with  $n$ , the value of  $L(n)$  will tend to a fraction of the area under the envelope function as  $n$  increases, resulting in the plateauing of  $L(n)$ , as clearly seen in Fig. 4(a), where  $L(n)$  results for five different values of  $U/\Gamma = 16.7, 13.9, 10.0, 6.25,$  and  $4.17$  are shown, for  $U = 1.25$ . The multiplicative factors shown on the right side of panel (a) were used to narrow the window in the vertical axis and improve visualization. As mentioned above, and easily observed for these results,  $L(n)$  plateaus as  $n$  increases. We define  $\xi_K^L$ , for each value of  $\Gamma$ , as the value of  $n$  for which we obtain the best collapse of the normalized  $L(n)$ , namely  $L(n)/L_{\text{max}}$ , as a function of  $n/\xi_K^L$ . The result of the collapse is shown in panel (b), and the values obtained for  $\xi_K^L$  are shown as black stars in

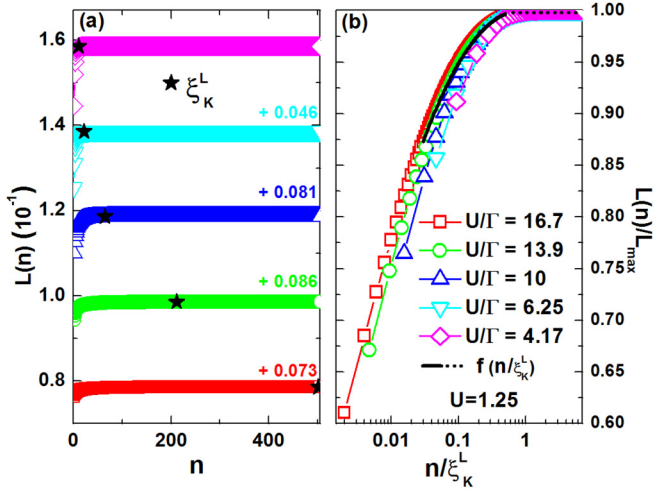


FIG. 4. (a) Function  $L(n)$ , obtained through Eq. (7), calculated for  $4.17 \leq U/\Gamma \leq 16.7$ , as indicated in the legend in (b), and  $U = 1.25$ . The scale  $\xi_K^L$  (marked by a black star) corresponds to the value of  $n$  for which the normalized  $L(n)/L_{\max}$  vs  $n/\xi_K^L$  curves collapse into a universal curve [see (b)]. The factors indicated on the right side of panel (a) were used to narrow the window in the vertical axis and improve the visualization of the data. (b) Semilogarithmic plot of  $L(n)/L_{\max}$ , the normalized  $L(n)$  curves from (a), as a function of  $n/\xi_K^L$ , showing their collapse into a universal curve  $f(n/\xi_K^L)$  (black solid and dotted lines).

Fig. 4(a). Figure 4(b) shows a semi-log plot of  $L(n)/L_{\max}$  vs  $n/\xi_K^L$ , confirming that all the normalized  $L(n)$  curves in panel (a) collapse perfectly into a single universal curve denoted  $f(n/\xi_K^L)$  (black solid and dotted lines) and characterized by a length scale that, from now on, we will refer to as  $\xi_K^L$  to indicate that it was obtained through LDOS calculations, using the  $L(n)$  function. The functional form of the universal curve shown in Fig. 4(b) is given by  $f(n/\xi_K^L) = \alpha \ln(n/\xi_K^L) + \beta \ln^2(n/\xi_K^L) + \gamma$  [solid black line in Fig. 4(b)], where  $\alpha = 1.39 \times 10^{-1}$ ,  $\beta = -1.15 \times 10^{-2}$ , and  $\gamma = 0.58$ , while  $f(n/\xi_K^L) \simeq 1.0$  once  $n/\xi_K^L \gtrsim 1.0$  [dotted black line in Fig. 4(b)]. In agreement with the discussion around Fig. 6, the universality occurs only after a certain distance from the impurity, which depends on the value of  $U/\Gamma$ .

#### IV. KONDO CLOUD EXTENSION OBTAINED THROUGH SPIN CORRELATIONS

The second method, which is more traditional [69–71], is based on the calculation of the spin-spin correlations  $\vec{S}_d \cdot \vec{S}_n$  between the impurity spin  $\vec{S}_d$  and the conduction electron spin  $\vec{S}_n$  at the  $n^{\text{th}}$  site, located inside the semi-infinite chain. In this context, the screening length  $\xi_K$  of the Kondo cloud is extracted from  $\vec{S}_d \cdot \vec{S}_n$  through the following procedure. Considering the integrated spin correlation function  $\Sigma(N) = \sum_{n=1}^N \langle \vec{S}_d \cdot \vec{S}_n \rangle$ —where  $n$  runs over the sites inside the semi-infinite chain and  $\langle \dots \rangle$  represents an average taken in the ground state—a certain value for  $\Sigma(N)$  will be chosen (see below) to define the Kondo cloud screening length  $\xi_K = N$  [78]. This method depends on developing a way to calculate  $\langle \vec{S}_d \cdot \vec{S}_n \rangle$ . As the finite- $U$  SBMFA is a mean-field procedure, it results in a one-body effective model with renormalized

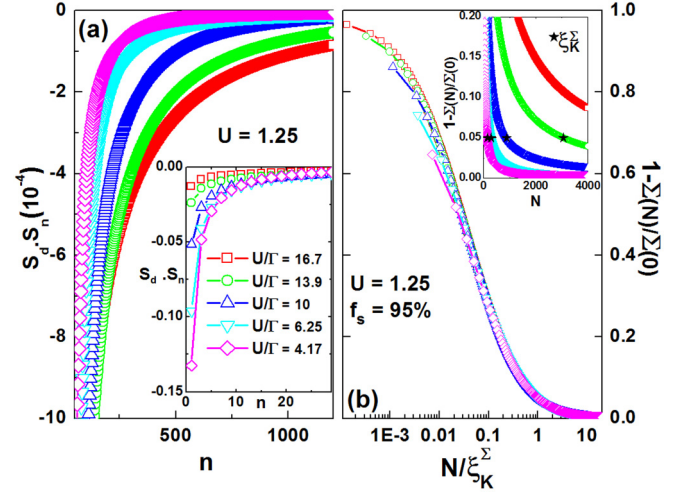


FIG. 5. (a) Spin-spin correlations  $\langle \vec{S}_d \cdot \vec{S}_n \rangle$  between the impurity and the conduction electron in the  $n^{\text{th}}$  site inside the chain for  $U = 1.25$  and different values of  $U/\Gamma$ , as indicated in the inset legend (same values as in Fig. 4). The inset shows a zoom for  $n < 30$ . Note that only results for odd values of  $n$  are shown, as  $\langle \vec{S}_d \cdot \vec{S}_n \rangle$  vanishes for even  $n$ . (b) Semilogarithmic plot of  $1 - \Sigma(N)/\Sigma(0)$  as a function of  $N/\xi_K^\Sigma$ , for  $U = 1.25$  and same values of  $U/\Gamma$  as in (a). Note the very good collapse of the curves (aside from a region around the impurity), indicating their universality. The inset shows how the  $\xi_K^\Sigma$  values (indicated as black stars, except for the (red) squares curve, which falls outside the range shown) used to collapse the curves in the main panel were obtained:  $\xi_K^\Sigma$  is the value of  $N$  for which the sum  $\Sigma(N)$  reaches  $f_s = 95\%$  of  $\Sigma(0) = -\langle \vec{S}_d^2 \rangle$ , i.e.,  $\xi_K^\Sigma$  is the distance from the impurity for which 95% of the impurity’s magnetic moment is screened by the conduction electrons that form a singlet with the impurity.

coupling  $\tilde{\Gamma}$  and impurity energy level  $\tilde{\epsilon}_d$ , with the first being dependent on a renormalization factor  $z$  and the second on a Lagrange multiplier  $\lambda$ , which are self-consistently obtained using the finite- $U$  SBMFA. Therefore, to calculate  $\langle \vec{S}_d \cdot \vec{S}_n \rangle$ , for the renormalized Hamiltonian, we will use the one-body expression [71]

$$\langle \vec{S}_d \cdot \vec{S}_n \rangle = \frac{3}{2} \langle c_d^\dagger c_n \rangle (\delta_{dn} - \langle c_n^\dagger c_d \rangle), \quad (8)$$

where the EOM was used to obtain  $\langle c_d^\dagger c_n \rangle$  and its Hermitian conjugate [79]. In addition, notice that, given the  $SU(2)$  symmetry of the problem, the  $c_d$  and  $c_n$  operators refer to either spin up or spin down. Notice that a full justification of the use of Eq. (8) is provided in the last two paragraphs of this section, including the results in Fig. 7.

The Kondo screening length obtained using spin correlations, from now on denoted as  $\xi_K^\Sigma$ , will be defined as the value of  $N$  for which  $\Sigma(N)$  reaches a determined percentage of  $\Sigma(0) = -\langle \vec{S}_d^2 \rangle$ , i.e., the negative of the square of the impurity spin to be screened [78], as originally proposed in Refs. [69–71,80,81]. We will call the percentage used to determine  $\xi_K^\Sigma$  as the shielding factor, and denote it by  $f_s$ . Thus we will define the screening length  $\xi_K^\Sigma$  as the value of  $N$  for which  $\Sigma(N)$  equals  $f_s = 95\%$  of  $-\langle \vec{S}_d^2 \rangle$ . In other words, when the quantity  $1 - \Sigma(N)/\Sigma(0)$  reaches the value 0.05 [see the inset in Fig. 5(b)]. In qualitative terms, this is equivalent

to stating that  $f_s = 95\%$  of the Kondo cloud is contained within a distance  $\xi_K^\Sigma$  from the impurity, or, equivalently, the distance from the impurity for which 95% of the Kondo singlet is formed. Or, lastly, if one pictures a conduction electron forming a singlet with the impurity, the extent of its wave function is approximately  $\xi_K^\Sigma$ . Therefore, for  $f_s = 95\%$ , the distance  $\xi_K^\Sigma$ , when measured from the impurity, effectively defines the edge of the Kondo cloud.

The results obtained through the spin correlations method are presented in Fig. 5. Panel (a) shows  $\langle \vec{S}_d \cdot \vec{S}_n \rangle$  results for  $4.17 \leq U/\Gamma \leq 16.7$ , with  $U = 1.25$ . Notice that, as these results are for an effective noninteracting model, all even- $n$  results vanish, therefore only odd- $n$  results are shown. As expected, the magnitude of  $\langle \vec{S}_d \cdot \vec{S}_n \rangle$ , for  $n$  close to the impurity [see the inset to panel (a)], starts at large values and rapidly approaches zero as  $n$  increases. Again, note that the negative values for these correlations reflect the fact that only results for odd  $n$  are shown. In addition, close to the impurity [inset in Fig. 5(a)], larger values of  $\Gamma$  (smaller values of  $U/\Gamma$ ) result in larger values (in magnitude) of  $\langle \vec{S}_d \cdot \vec{S}_n \rangle$ , as one expects to obtain larger effective Kondo exchanges ( $J_K$ ) for larger  $\Gamma$  values at fixed  $U$ . As a consequence, one also expects that  $\langle \vec{S}_d \cdot \vec{S}_n \rangle$  will approach zero faster for larger  $\Gamma$  as  $n$  increases (see main panel). Therefore, at fixed  $U$ , a larger  $\Gamma$ , which also leads to a larger Kondo temperature  $T_K$ , leads to a smaller Kondo cloud. We then have the well known rule of thumb stating that as the Kondo temperature increases, the Kondo cloud decreases, a result encoded in Eq. (1).

In the inset to Fig. 5(b), we show  $1 - \Sigma(N)/\Sigma(0)$  results for  $U = 1.25$  and the same  $U/\Gamma$  values as in panel (a). The intersection of the horizontal dotted line (at 0.05) with the different curves indicates the values of  $N$  for which the sum  $\Sigma(N) = \sum_{n=1}^N \langle \vec{S}_d \cdot \vec{S}_n \rangle$  reaches  $f_s = 95\%$  of  $\Sigma(0) = -\langle \vec{S}_d^2 \rangle$ , and therefore results in  $1 - \Sigma(N)/\Sigma(0) = 0.05$ . We take the value of  $N$  at the intercept as an estimate of  $\xi_K^\Sigma$  for each  $\Gamma$ , marking them with black stars. In the main panel of Fig. 5(b), we show a semilogarithmic plot of  $1 - \Sigma(N)/\Sigma(0)$  versus  $N/\xi_K^\Sigma$ , using the  $\xi_K^\Sigma$  values as obtained in the inset. These results clearly show that the decay of  $1 - \Sigma(N)/\Sigma(0)$  follows a universal curve  $g(N/\xi_K^\Sigma)$  characterized by a length scale that, as mentioned above, we will refer to as  $\xi_K^\Sigma$ , indicating that it was obtained through the spin correlations procedure just described. Finally, it should be noted that using  $f_s < 95\%$ , thus resulting in smaller  $\xi_K^\Sigma$  values, produces collapsed curves that are very similar to the ones in the main panel of Fig. 5(b). This is not surprising, since the results in Fig. 5(b) already indicate that the integrated spin correlations are universal over a large region of the Kondo cloud. We compared results (not shown) for  $f_s$  values down to 70%, which results in screening lengths  $\xi_K^\Sigma$  that are very similar to the  $\xi_K^L$  values obtained through the LDOS method [Fig. 4(b)]. Therefore the  $L(n)$  method probes the Kondo cloud up to a distance from the impurity where just 70% of its localized magnetic moment has been screened by the conduction electrons. However, as just argued, since this region of the Kondo cloud already displays universal behavior, the LDOS and the spin correlations results for  $\xi_K$  provide compatible information, as discussed next.

It is interesting to note that the quality of the collapse of the curves in Figs. 4(b) and 5(b) is clearly degraded as one

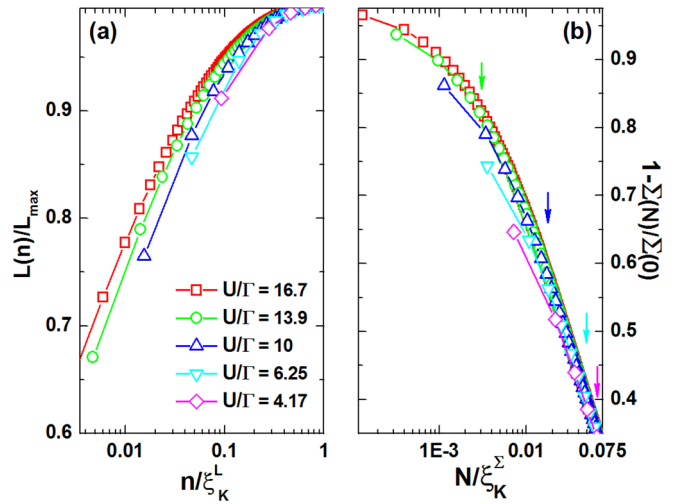


FIG. 6. (a) and (b) show a zoom of Figs. 4(b) and 5(b), respectively, at the region adjacent to the impurity up to the point where the data collapse into a universal curve. The arrows in (b) approximately indicate the point where each curve, starting with the one for  $U/\Gamma = 4.17$  [(magenta) diamonds], starts to deviate from the others (i.e., the point where the free orbital region starts, see text). Note that in (a) we are not showing the data for even sites to facilitate the comparison with data in (b).

approaches the impurity. Motivated by this, and by previous results in Ref. [66], we believe that this loss of universality may be connected to the presence of a region around the impurity (associated to the free orbital fixed point [66]) where physical quantities that depend on the distance from the impurity, like  $L(n)$  and  $\Sigma(N)$ , do not follow anymore the universal scaling functions,  $f(n/\xi_K^L)$  and  $g(N/\xi_K^\Sigma)$ , that were obtained at regions progressively closer to the edge of the Kondo cloud. This loss of universality can be seen in more detail in Fig. 6, where panels (a) and (b) show a zoom of the data in Figs. 4(b) and 5(b), respectively, at the region adjacent to the impurity up to the point where the  $L(n)/L_{\max}$  and  $1 - \Sigma(N)/\Sigma(0)$  data start to follow their corresponding universal curves. It is important to note that the rightmost point in the horizontal axis in both panels in Fig. 6, i.e.,  $n/\xi_K^L = 1$  and  $N/\xi_K^\Sigma = 0.075$  are at approximately the same distance from the impurity. This can be easily verified by counting the number of symbols from the beginning of each curve up to the rightmost edge of each panel [notice that in panel (a) we removed the even site symbols to facilitate the comparison with panel (b)]. A comparison of both panels shows that the loss of universality in the LDOS and spin correlation probes of the Kondo cloud are qualitatively similar, indicating that they are providing similar information, as can be confirmed in Fig. 8 by noticing the very good agreement in the dependence of  $\xi_K^\Sigma$  and  $\xi_K^L$  with  $U/\Gamma$ . Finally, the data in Fig. 6 do not lend itself to an easy quantitative analysis of the so-called free orbital region [66] around the impurity. However, the data clearly show that the ratio between the size of this putative central region and the total size of the Kondo cloud decreases sharply as  $U/\Gamma$  increases. This is indicated by the vertical arrows in Fig. 6(b), which roughly mark the point where each curve starts to deviate from the others (i.e., the point where the free

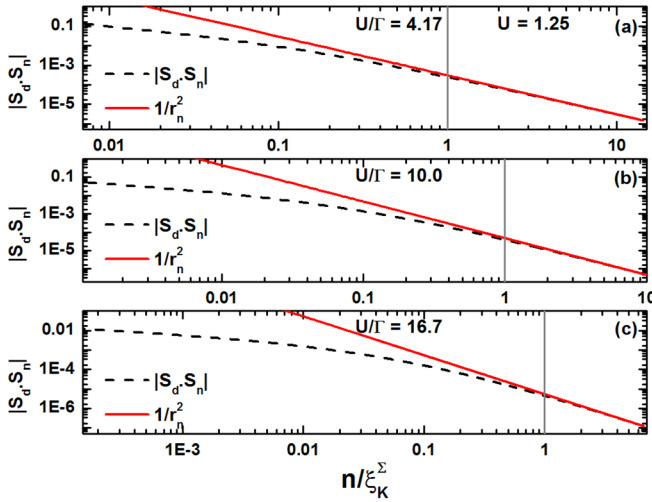


FIG. 7. Log-log plot of  $|\vec{S}_d \cdot \vec{S}_n|$  (dashed black curves) as a function of  $n/\xi_K^\Sigma$  for  $U/\Gamma = 4.17, 10.0,$  and  $16.7$  in (a) to (c). All results for  $U = 1.25$ . The gray (red) solid curves are  $\propto 1/r_n^2$ , with a proportionality constant chosen so that it matches the spin correlation calculated for the largest value of  $n$ , and  $r_n$  is the distance to the impurity. The comparison of the two curves clearly indicates that the spin correlations decay as the second power of distance to the impurity *outside* of the cloud, as defined by  $\xi_K^\Sigma$ .

orbital region starts for each value of  $U/\Gamma$ , beginning with the  $U/\Gamma = 4.17$  curve [(magenta) diamonds], up to the  $U/\Gamma = 13.9$  curve [(green) circles]. The position of these arrows allows us to roughly estimate that the ratio between the size of the free orbital region and the size of the Kondo cloud decreases by more than one order of magnitude as we approximately triple  $U/\Gamma$ . This is in qualitative agreement with the results shown in the bottom panel of Fig. 2 in Ref. [66].

Before proceeding to a comparison of the  $\xi_K$  results obtained through  $L(n)$  and  $\Sigma(N)$ , in Figs. 4 and 5, respectively, we wish to clarify a possibly contentious point regarding the approximation we have taken. Note that, as mentioned above, Eq. (8) is the expression one obtains for the spin correlations when  $U = 0$ . This does not mean that our results were obtained for  $U = 0$  in Eq. (3). In reality, what this means is that the SBMFA, being a mean-field technique, when applied to the SIAM, results in a one-body effective model, where the correlation effects are taken care of by the self-consistent renormalization factors  $z$  and  $\lambda$ , which depend on  $U$  and  $\Gamma$ . Thus the  $U = 0$  expression for the spin correlations [Eq. (8)] is the appropriate one to be used, as the resulting effective model is a *renormalized*  $U = 0$  model. However, exactly because of that, it is not at all obvious that the use of this (uncorrelated) one-body equation to calculate the spin correlations will provide accurate information about the Kondo state, which is highly correlated. The results just shown in Fig. 5 (and later on, in Fig. 8) provide indirect evidence in support of our approach to calculate the spin correlations using the SBMFA. Indeed, the universality of the curves in the main panel of Fig. 5(b), and the fact that the  $\xi_K^\Sigma$  extracted from it have the expected dependence with  $U/\Gamma$  (see Fig. 8), are quite reassuring. Figure 7 provides further support to the approach we have taken: the magnitude of the spin correlations for odd

sites (dashed curve), since those for even sites vanish, for three different values of  $U/\Gamma = 4.17, 10.0,$  and  $16.7$  [panels (a) to (c)], behaves as  $1/r_n^2$  [solid (red) curve], *outside* of the Kondo cloud (i.e., for  $r_n \gtrsim \xi_K^\Sigma$ ), where  $r_n$  is the distance from the impurity. This is the expected behavior for the spin correlations in the Kondo state as predicted by Fermi-liquid theory [16,68]. In summary, the very good agreement between the calculated spin correlations (dashed curve) for  $r_n \gtrsim \xi_K^\Sigma$  (to the right of the dashed vertical line) and the  $\propto 1/r_n^2$  curve (solid line), where the  $\xi_K^\Sigma$  values used are the ones obtained in Fig. 5, adds extra support to the results obtained.

Two additional points regarding the use of Eq. (8) should be discussed in more detail. First, as mentioned above,  $\langle \vec{S}_d \cdot \vec{S}_n \rangle = 0$  for even- $n$  sites, i.e., the corresponding ferromagnetic correlations, obtained at even- $n$  sites for finite  $U$ , vanish when Eq. (8) is used. At first sight, this may throw into question the results for  $\Sigma(N)$ . However, as can be checked in Ref. [71], the finite- $U$  ferromagnetic correlations for even- $n$  have a much smaller magnitude than the antiferromagnetic correlations for odd- $n$  sites. In addition, the ferromagnetic correlations also decay much faster than the antiferromagnetic ones. Therefore the integrated spin correlation function  $\Sigma(N)$ , obtained through the use of Eq. (8), will deviate quantitatively from its exact value just for  $N$  values that are very close to the impurity (see left panel of Fig. 3 in Ref. [71]). It is also interesting to note that for the Kondo model, the ferromagnetic correlations, present in the Anderson impurity model, vanish. This can be observed in Fig. 2 of Ref. [16].

Second, the use of Eq. (8) for the  $U = 0$  effective model results in  $\langle S_d^2 \rangle = 3/8$ , thus  $\Sigma(\xi_K^\Sigma) \approx -3/8$ . It can be shown (see below) that the corresponding finite- $U$  results (at the particle-hole symmetric point and deep inside the Kondo regime) are, very approximately,  $3/4$  and  $-3/4$ , respectively. The  $1/2$  multiplicative factor in the results obtained from Eq. (8) can be intuitively understood by solving a toy model comprised of two  $U = 0$  sites, where one of the sites represents the impurity, the other plays the role of the “chain,” and they are coupled by an overlap integral  $t'$ . The ground state of this toy model is given by

$$|GS\rangle_{U=0} = \frac{1}{2} [|\uparrow, \downarrow\rangle - |\downarrow, \uparrow\rangle + |\uparrow\downarrow, 0\rangle + |0, \uparrow\downarrow\rangle], \quad (9)$$

where  $\uparrow$  and  $\downarrow$  indicate spin up and spin down, respectively, and we use the notation  $|\text{site 1, site 2}\rangle$ . It is straightforward to show that for this ground state  $\langle S_1^2 \rangle = 3/8$  and  $\langle \vec{S}_1 \cdot \vec{S}_2 \rangle = -3/8$ , as the singlet comprises just half of the ground state, which now also contains double occupied and empty sites contributions. Nevertheless, the localized spin in the impurity (site 1) will be perfectly screened by the antiferromagnetic correlations, between sites 1 and 2, inside the “Kondo cloud.” The same toy model, but now with finite  $U$  on site 1, results in a ground state given by

$$|GS\rangle_U = \frac{(1 + \beta^2)^{-\frac{1}{2}}}{\sqrt{2}} [|\uparrow, \downarrow\rangle - |\downarrow, \uparrow\rangle + \beta (|\uparrow\downarrow, 0\rangle + |0, \uparrow\downarrow\rangle)], \quad (10)$$

where  $\beta = 4t'/U$ , which becomes vanishingly small deep inside the Kondo regime, removing the double occupied states, thus  $\langle S_1^2 \rangle \approx 3/4$  and  $\langle \vec{S}_1 \cdot \vec{S}_2 \rangle \approx -3/4$ , as mentioned above.

In addition, it is interesting to note that, for a toy model like the one just described, but where  $U \rightarrow \infty$  and the impurity level is at the “Fermi energy” ( $\epsilon_1 = 0$ ), the ground state is given by

$$|\text{GS}\rangle_{U \rightarrow \infty} = \frac{1}{\sqrt{2}} \left[ \frac{1}{\sqrt{2}} (|\uparrow, \downarrow\rangle - |\downarrow, \uparrow\rangle) + |0, \uparrow\downarrow\rangle \right], \quad (11)$$

where, as for the  $U = 0$  case,  $\langle \vec{S}_1^2 \rangle = 3/8$  and  $\langle \vec{S}_1 \cdot \vec{S}_2 \rangle = -3/8$ . This  $U \rightarrow \infty$  toy model can be slightly modified to provide more information regarding this issue: one can move the impurity level below the Fermi energy ( $\epsilon_1 < 0$ ), and in this case, if  $8t^2/\epsilon_1^2 \ll 1$ , the ground state, to first order in  $t^2/\epsilon_1^2$ , is given by

$$|\text{GS}\rangle_{U \rightarrow \infty} \approx (1 + \alpha)^{-\frac{1}{2}} |s\rangle + (1 + \alpha^{-1})^{-\frac{1}{2}} |0, \uparrow\downarrow\rangle \quad (12)$$

where  $\alpha = \gamma/(1+\gamma)^2$ ,  $\gamma = 2t^2/\epsilon_1^2$ , and  $|s\rangle = 1/\sqrt{2}(|\uparrow, \downarrow\rangle - |\downarrow, \uparrow\rangle)$ . For this ground state, we have that  $\langle \vec{S}_1^2 \rangle = (1 + \alpha)^{-1} 3/4$ , which is  $\approx 3/4$ , if  $\gamma \ll 1$  (with  $\langle \vec{S}_1 \cdot \vec{S}_2 \rangle = -\langle \vec{S}_1^2 \rangle$ ). Thus, by varying  $\epsilon_1$  from the Fermi energy to deep below it, and keeping the system in Kondo while doing it, we have that  $3/4 \gtrsim \langle \vec{S}_1^2 \rangle \geq 3/8$  (with  $\langle \vec{S}_1 \cdot \vec{S}_2 \rangle = -\langle \vec{S}_1^2 \rangle$ ). Therefore this infinite- $U$  toy model suggests that one can cover the whole  $3/8$  to  $3/4$  range by suitably adjusting the  $\epsilon_1$  and  $t'$  parameters, while staying inside the Kondo regime, with full screening of the impurity. This illustrates what was stated above, i.e., that the most relevant is not the specific value of  $\langle \vec{S}_d^2 \rangle$ , but that there is screening of the localized moment.

The two points just argued above, together with the good universal collapse shown in Fig. 5(b), the indications of an internal structure of the Kondo cloud presented in Fig. 6(b), the asymptotic behavior of the spin correlations (for different values of  $U/\Gamma$ ) shown in Fig. 7, and the agreement with the expected dependence of  $\xi_K^\Sigma$  versus  $U/\Gamma$  (see Fig. 8), leads us to believe that Eq. (8) captures the main features of the spin correlations inside the Kondo cloud.

In conclusion, it should also be noted that there are a couple of advantages in using this procedure to calculate the spin correlations. First, once the renormalized one-body model is obtained through SBMFA, there are no further approximations to be done, neither analytical [as Eq. (8) is exact], nor numerical, as the spin correlations can be obtained to any distance from the impurity with machine-precision accuracy. Therefore, contrary to the use of DMRG to calculate spin correlations (see, for example, Ref. [70]), which can only be done in finite clusters, we do not have to deal with finite-size effects in our calculations. Second, and quite importantly, since the spin correlations for  $U = 0$  at even sites vanish, contrary to the spin correlations for a finite- $U$  model, which are ferromagnetic (see, for example, Refs. [70,71]), our  $\Sigma(N)$  turns out to be monotonic, instead of oscillating with  $N$ , as is the case for the DMRG calculations [70]. As discussed in Ref. [70], this makes the universal collapse of the  $1 - \Sigma(N)/\Sigma(0)$  functions rather more difficult, which, added to the finite-size effects intrinsic to DMRG, increases the uncertainty of the DMRG  $\xi_K$  results. Our use of Eq. (8) eliminates all of these problems, as can be seen from the very nice collapse obtained in Fig. 5(b), aside from a region around the impurity.

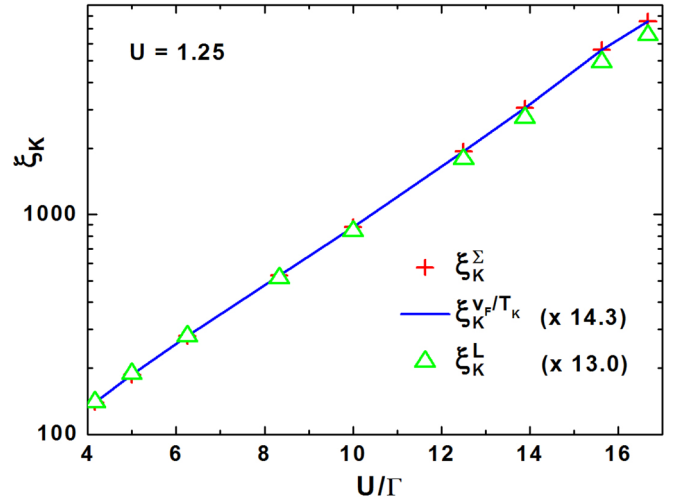


FIG. 8. Semilogarithmic plot of the Kondo screening length  $\xi_K$ , as a function of  $U/\Gamma$ , obtained through  $v_F/T_K$  [(blue) solid line], the  $L(n)$  function [(green) triangles], and through the  $\Sigma(N)$  spin correlations method [(red) plus signs]. The first two were multiplied by a scaling factor (as indicated in the legend) to facilitate the comparison. Note that  $v_F = 2.0$  and  $T_K$  was obtained through the finite- $U$  SBMFA.

## V. COMPARISON OF THE RESULTS OBTAINED BY THE TWO METHODS

Figure 8 presents the results obtained by both methods. In it we see a semilogarithmic plot of  $\xi_K$ , obtained in three different ways, as a function of  $U/\Gamma$  in the interval [4.0; 17.0]. The light-gray (red) plus-sign curve shows results for the Kondo cloud screening length  $\xi_K^\Sigma$  obtained through spin correlations, while the gray (green) triangles curve shows results for the Kondo length scale  $\xi_K^L$  obtained through LDOS. The dark (blue) solid curve shows results for the Kondo cloud extension  $\xi_K^{v_F/T_K}$ , calculated using Eq. (1), where  $T_K$  is the width of the Kondo peak obtained by the finite- $U$  SBMFA and  $v_F = 2.0$  is the Fermi velocity. The results for the last two are multiplied by scaling factors (as indicated in the legend) to facilitate comparison. On one hand, the results clearly show that  $\xi_K^\Sigma$  [(red) plus signs] is quantitatively indistinguishable from  $\xi_K^{v_F/T_K}$  [(blue) solid line] for the whole  $U/\Gamma$  range. On the other hand, the results for  $\xi_K^L$  [(green) triangles] show some slight deviation in relation to the other two; it displays very small quantitative differences in the  $U/\Gamma$  region closer to the charge fluctuation regime, while there is a small quantitative difference once one gets deeper into the Kondo regime region, where the slope of the  $\xi_K^L$  curve becomes slightly smaller than the one for the other two curves. The overall quantitative agreement between the  $\xi_K^L$  and  $\xi_K^\Sigma$  results further validates the LDOS approach as *complementary* to the spin correlations one, as it independently gathers information on the region adjacent to the impurity, showing the same loss of universality, in qualitative agreement with the results in Ref. [66]. In addition, the agreement with the  $v_F/T_K$  results serves as an *a posteriori* validation of this heuristic estimate of the Kondo cloud extension. Finally, as an additional comparison, Fig. 5 in Ref. [63] shows exponential scaling behavior, obtained for the Kondo model when using entanglement tools such as

concurrence, in good qualitative agreement with our results in Fig. 8.

In summary, the use of two different numerical techniques to estimate the Kondo cloud extension, using the finite-U SBMFA, allowed us to make a few interesting observations. First, regarding the extension of the Kondo cloud, obtained through  $\xi_K^\Sigma$  (using a shielding factor  $f_s = 95\%$ ), we showed that its dependence with  $U/\Gamma$  is quantitatively indistinguishable from the expected  $v_F/T_K$  behavior. By using a technique that is free from finite size effects, as opposed to DMRG [70,71], we were able to analyze results much deeper into the Kondo regime. In addition, the lack of oscillations in  $\Sigma(N)$  [70] unveiled a systematic loss of universality close to the impurity, which may be an indication of the existence of an internal structure in the Kondo cloud, previously observed with NRG [66]. A qualitatively similar loss of universality in the  $L(n)$  results gives support to this interpretation. Indeed, the agreement in the loss of universality between spin correlations and LDOS shown in Fig. 6, which points to a possible internal structure of the Kondo cloud, and the agreement between the spin and charge sectors also shown in Fig. 8, seem an indication that Eq. (7) captures, through the LDOS, the essential scaling properties of the Kondo cloud in the charge sector. The authors believe that the results here presented, which partially uncover the Kondo cloud's internal structure, provide an additional step in the direction of determining ways to experimentally probe this most elusive concept.

#### ACKNOWLEDGMENTS

The authors are grateful to E. Vernek for fruitful discussions on the subject matter of this work and to the authors of Ref. [71] for providing the numerical results for their Fig. 3. This work has been supported by the Brazilian agencies FAPERJ, under Grant No. 2015048000 (G.G.S.), and CNPq, under Grants No. 141134/2015-1 (G.G.S.) and No. 306000/2017-2 (E.V.A.).

#### APPENDIX: FINITE-U SLAVE BOSON MEAN-FIELD APPROXIMATION

The slave boson mean-field approximation was originally proposed to treat systems where the Coulomb repulsion  $U$  is the dominant parameter, which was then taken as being infinity. [82] Therefore double occupancy states were removed from the Hilbert space with the help of projection operators that include auxiliary bosonic operators, which are

then replaced with their mean-field value (calculated self-consistently). Thus the many-body Hamiltonian is mapped into an effective one-body Hamiltonian that can be solved exactly [82].

The so-called finite-U SBMFA is an extension of the usual slave boson mean-field that is appropriate to treat problems with finite  $U$  [72]. The first step in the approximation is to enlarge the Hilbert space by introducing a set of slave boson operators  $\hat{e}$ ,  $\hat{p}_\sigma$ , and  $\hat{d}$ , then replacing the creation  $d_\sigma^\dagger$  and annihilation  $d_\sigma$  operators in the Hamiltonian by  $\hat{d}^\dagger \hat{z}_\sigma^\dagger$  and  $\hat{z}_\sigma \hat{d}$ , respectively, where, following Kotliar and Rukenstein [72], the operator  $\hat{z}_\sigma$  takes the form

$$\hat{z}_\sigma = [1 - \hat{d}^\dagger \hat{d} - \hat{p}_\sigma^\dagger \hat{p}_\sigma]^{1/2} [\hat{e}^\dagger \hat{p}_\sigma + \hat{p}_\sigma^\dagger \hat{d}] \times [1 - \hat{e}^\dagger \hat{e} - \hat{p}_\sigma^\dagger \hat{p}_\sigma]^{1/2}. \quad (\text{A1})$$

Notice that the bosonic operators  $\hat{d}$  and  $\hat{d}^\dagger$  do not carry a spin index. The enlarged Hilbert space is then restricted to the physically meaningful subspace by imposing the constraints

$$\hat{P} = \hat{e}^\dagger \hat{e} + \sum_\sigma \hat{p}_\sigma^\dagger \hat{p}_\sigma + \hat{d}^\dagger \hat{d} - 1 = 0 \quad (\text{A2})$$

and

$$\hat{Q}_\sigma = n_{d\sigma} - \hat{p}_\sigma^\dagger \hat{p}_\sigma - \hat{d}^\dagger \hat{d} = 0. \quad (\text{A3})$$

Both constraints are included into the Hamiltonian through Lagrange multipliers denoted  $\lambda^{(1)}$  and  $\lambda_\sigma^{(2)}$ . The constraint in Eq. (A2) restricts the impurity to having states with only zero, single, or double occupancy, while Eq. (A3) relates the boson with the fermion occupancies. In the mean-field approximation, the boson operators  $\hat{e}$ ,  $\hat{p}_\sigma$ , and  $\hat{d}$  (as well as their Hermitian conjugates) are replaced by their thermodynamic expectation values  $e \equiv \langle \hat{e} \rangle = \langle \hat{e}^\dagger \rangle$ ,  $p_\sigma \equiv \langle \hat{p}_\sigma \rangle = \langle \hat{p}_\sigma^\dagger \rangle$ , and  $d \equiv \langle \hat{d} \rangle = \langle \hat{d}^\dagger \rangle$ . These expectation values, plus the Lagrange multipliers, constitute a set of parameters to be self-consistently determined by minimizing the total energy  $\langle H \rangle$ . Once again, as in the infinite  $U$  case, the many-body problem has been reduced to a one-body problem, whose energy can be easily minimized. The Green's function at the impurity, which is needed to calculate the LDOS at each chain-site, is given by

$$G_{dd}^\sigma = \langle \langle z_\sigma d_\sigma; d_\sigma^\dagger z_\sigma^\dagger \rangle \rangle, \quad (\text{A4})$$

which is the propagator that carries the correct weight of the Kondo resonance. Notice that in Ref. [6], the reader can find how to calculate the Green's function in the chain sites using  $G_{dd}^\sigma$  as an input to the equation of motion formalism. This is necessary to obtain the LDOS in the chain sites, which is then used in Eq. (7).

- 
- [1] J. Kondo, *Prog. Theor. Phys.* **32**, 37 (1964).  
 [2] A. C. Hewson, *The Kondo Problem to Heavy Fermions* (Cambridge University Press, Cambridge, 1993).  
 [3] D. Goldhaber-Gordon, H. Shtrikman, D. Mahalu, D. Abusch-Magder, U. Meirav, and M. Kastner, *Nature (London)* **391**, 156 (1998).  
 [4] I. Affleck, in *Perspectives of Mesoscopic Physics—Dedicated to Yoseph Imry's 70<sup>th</sup> Birthday*, edited by A. Aharony and O. Entin-Wohlman (World Scientific, Singapore, 2010), Chap. 1, pp. 1–44.  
 [5] E. S. Sørensen and I. Affleck, *Phys. Rev. B* **53**, 9153 (1996).  
 [6] C. A. Büsser, G. B. Martins, L. Costa Ribeiro, E. Vernek, E. V. Anda, and E. Dagotto, *Phys. Rev. B* **81**, 045111 (2010).  
 [7] N. Néel, R. Berndt, J. Kröger, T. O. Wehling, A. I. Lichtenstein, and M. I. Katsnelson, *Phys. Rev. Lett.* **107**, 106804 (2011).  
 [8] Y. Nishida, *Phys. Rev. Lett.* **111**, 135301 (2013).  
 [9] J. Bauer, C. Salomon, and E. Demler, *Phys. Rev. Lett.* **111**, 215304 (2013).  
 [10] I. Snyman and S. Florens, *Phys. Rev. B* **92**, 085131 (2015).

- [11] W. J. De Haas and G. J. Van Den Berg, *Physica* **3**, 440 (1936).
- [12] J. B. Boyce and C. P. Slichter, *Phys. Rev. Lett.* **32**, 61 (1974).
- [13] J. B. Boyce and C. P. Slichter, *Phys. Rev. B* **13**, 379 (1976).
- [14] NMR research prior to the measurements described in Refs. [12,13] can be found in A. J. Heeger, L. B. Welsh, M. A. Jensen, and G. Gladstone, *Phys. Rev.* **172** 302 (1968), as well as in D. C. Golibersuch and A. J. Heeger, *ibid.* **182**, 584 (1969). In this latter paper, a survey of Mössbauer results on CuFe, related to the Kondo cloud, is also presented.
- [15] G. Bergmann, *Phys. Rev. B* **77**, 104401 (2008).
- [16] L. Borda, *Phys. Rev. B* **75**, 041307 (2007).
- [17] H. Manoharan, C. Lutz, and D. Eigler, *Nature (London)* **403**, 512 (2000).
- [18] J. Li, W.-D. Schneider, R. Berndt, and B. Delley, *Phys. Rev. Lett.* **80**, 2893 (1998).
- [19] V. Madhavan, W. Chen, T. Jamneala, M. F. Crommie, and N. S. Wingreen, *Science* **280**, 567 (1998).
- [20] V. Madhavan, W. Chen, T. Jamneala, M. F. Crommie, and N. S. Wingreen, *Phys. Rev. B* **64**, 165412 (2001).
- [21] N. Knorr, M. A. Schneider, L. Diekhöner, P. Wahl, and K. Kern, *Phys. Rev. Lett.* **88**, 096804 (2002).
- [22] M. A. Schneider, L. Vitali, N. Knorr, and K. Kern, *Phys. Rev. B* **65**, 121406 (2002).
- [23] N. Quaas, M. Wenderoth, A. Weismann, R. G. Ulbrich, and K. Schönhammer, *Phys. Rev. B* **69**, 201103 (2004).
- [24] A. Zhao, Q. Li, L. Chen, H. Xiang, W. Wang, S. Pan, B. Wang, X. Xiao, J. Yang, J. G. Hou, and Q. Zhu, *Science* **309**, 1542 (2005).
- [25] M. Schneider, L. Vitali, P. Wahl, N. Knorr, L. Diekhöner, G. Wittich, M. Vogelgesang, and K. Kern, *Appl. Phys. A* **80**, 937 (2005).
- [26] V. Iancu, A. Deshpande, and S.-W. Hla, *Nano Lett.* **6**, 820 (2006).
- [27] N. Néel, J. Kröger, L. Limot, K. Palotas, W. A. Hofer, and R. Berndt, *Phys. Rev. Lett.* **98**, 016801 (2007).
- [28] N. Néel, J. Kröger, R. Berndt, T. O. Wehling, A. I. Lichtenstein, and M. I. Katsnelson, *Phys. Rev. Lett.* **101**, 266803 (2008).
- [29] A. Gumbsch, G. Barcaro, M. G. Ramsey, S. Surnev, A. Fortunelli, and F. P. Netzer, *Phys. Rev. B* **81**, 165420 (2010).
- [30] H. Prüser, M. Wenderoth, P. E. Dargel, A. Weismann, R. Peters, T. Pruschke, and R. G. Ulbrich, *Nat. Phys.* **7**, 203 (2011).
- [31] H. Prüser, M. Wenderoth, A. Weismann, and R. G. Ulbrich, *Phys. Rev. Lett.* **108**, 166604 (2012).
- [32] S. Meierott, N. Néel, and J. Kröger, *Phys. Rev. B* **91**, 201111 (2015).
- [33] M. Ternes, A. J. Heinrich, and W.-D. Schneider, *J. Phys.: Condens. Matter* **21**, 053001 (2009).
- [34] O. Újsághy, J. Kroha, L. Szunyogh, and A. Zawadowski, *Phys. Rev. Lett.* **85**, 2557 (2000).
- [35] A. Schiller and S. Hershfield, *Phys. Rev. B* **61**, 9036 (2000).
- [36] M. Plihal and J. W. Gadzuk, *Phys. Rev. B* **63**, 085404 (2001).
- [37] U. Fano, *Phys. Rev.* **124**, 1866 (1961).
- [38] J. Merino and O. Gunnarsson, *Phys. Rev. B* **69**, 115404 (2004).
- [39] A. Weismann, M. Wenderoth, S. Lounis, P. Zahn, N. Quaas, R. G. Ulbrich, P. H. Dederichs, and S. Blügel, *Science* **323**, 1190 (2009).
- [40] H. T. Dang, M. dos Santos Dias, A. Liebsch, and S. Lounis, *Phys. Rev. B* **93**, 115123 (2016).
- [41] The term ‘Kondo-box’ was used for the first time by; W. B. Thimm, J. Kroha, and J. von Delft, *Phys. Rev. Lett.* **82**, 2143 (1999).
- [42] P. Simon and I. Affleck, *Phys. Rev. Lett.* **89**, 206602 (2002).
- [43] P. Simon and I. Affleck, *Phys. Rev. B* **68**, 115304 (2003).
- [44] P. S. Cornaglia and C. A. Balseiro, *Phys. Rev. Lett.* **90**, 216801 (2003).
- [45] J. Park, S.-S. B. Lee, Y. Oreg, and H.-S. Sim, *Phys. Rev. Lett.* **110**, 246603 (2013).
- [46] B. A. Bernevig, T. L. Hughes, and S.-C. Zhang, *Science* **314**, 1757 (2006).
- [47] M. König, S. Wiedmann, C. Brüne, A. Roth, H. Buhmann, L. W. Molenkamp, X.-L. Qi, and S.-C. Zhang, *Science* **318**, 766 (2007).
- [48] M. König, H. Buhmann, L. W. Molenkamp, T. Hughes, C. X. Liu, X. L. Qi, and S. C. Zhang, *J. Phys. Soc. Jpn.* **77**, 031007 (2008).
- [49] T. Posske, C.-X. Liu, J. C. Budich, and B. Trauzettel, *Phys. Rev. Lett.* **110**, 016602 (2013).
- [50] T. Posske and B. Trauzettel, *Phys. Rev. B* **89**, 075108 (2014).
- [51] N. Laflorencie, *Phys. Rep.* **646**, 1 (2016).
- [52] K. Yosida, *Phys. Rev.* **147**, 223 (1966).
- [53] S. Oh and J. Kim, *Phys. Rev. B* **73**, 052407 (2006).
- [54] E. S. Sørensen, M.-S. Chang, N. Laflorencie, and I. Affleck, *J. Stat. Mech.* (2007) P08003.
- [55] E. S. Sørensen, M.-S. Chang, N. Laflorencie, and I. Affleck, *J. Stat. Mech.* (2007) L01001.
- [56] I. Affleck, N. Laflorencie, and E. S. Sørensen, *J. Phys. A* **42**, 504009 (2009).
- [57] N. Laflorencie, E. Sørensen, and I. Affleck, *J. Stat. Mech.* (2008) P02007.
- [58] H. Frahm and A. A. Zvyagin, *J. Phys.: Condens. Matter* **9**, 9939 (1997).
- [59] A. Bayat, P. Sodano, and S. Bose, *Phys. Rev. B* **81**, 064429 (2010).
- [60] P. Sodano, A. Bayat, and S. Bose, *Phys. Rev. B* **81**, 100412 (2010).
- [61] A. Bayat, S. Bose, P. Sodano, and H. Johannesson, *Phys. Rev. Lett.* **109**, 066403 (2012).
- [62] S.-S. B. Lee, J. Park, and H.-S. Sim, *Phys. Rev. Lett.* **114**, 057203 (2015).
- [63] C. Yang and A. E. Feiguin, *Phys. Rev. B* **95**, 115106 (2017).
- [64] R. Zheng, R.-Q. He, and Z.-Y. Lu, *arXiv:1803.03072*.
- [65] G. Yoo, S.-S. B. Lee, and H.-S. Sim, *Phys. Rev. Lett.* **120**, 146801 (2018).
- [66] A. K. Mitchell, M. Becker, and R. Bulla, *Phys. Rev. B* **84**, 115120 (2011).
- [67] T. A. Costi and G. Zaránd, *Phys. Rev. B* **59**, 12398 (1999).
- [68] H. Ishii, *J. Low Temp. Phys.* **32**, 457 (1978).
- [69] J. E. Gubernatis, J. E. Hirsch, and D. J. Scalapino, *Phys. Rev. B* **35**, 8478 (1987).
- [70] A. Holzner, I. P. McCulloch, U. Schollwöck, J. von Delft, and F. Heidrich-Meisner, *Phys. Rev. B* **80**, 205114 (2009).
- [71] M. Nuss, M. Ganahl, E. Arrigoni, W. von der Linden, and H. G. Evertz, *Phys. Rev. B* **91**, 085127 (2015).
- [72] G. Kotliar and A. E. Ruckenstein, *Phys. Rev. Lett.* **57**, 1362 (1986).
- [73] L. C. Ribeiro, E. Vernek, G. B. Martins, and E. V. Anda, *Phys. Rev. B* **85**, 165401 (2012).

- [74] To suppress the Kondo effect, one can either obtain a solution valid for  $T > T_K$ , by using for example the Hubbard-I approximation [83] or by decoupling the impurity from the chain (making  $t' = 0$ ). Our experience is that both methods provide quantitatively similar results for  $\xi_K$ . In this work, we adopt the latter strategy.
- [75] It should be emphasized that the EOM method used to calculate the Green's function at an arbitrary site  $n$  in the semi-infinite chain is exact, in the sense that no truncation of the chain of equations of motion is needed. This is explicitly shown in our previous work, Ref. [6]. Thus, once the Green's function at the impurity is calculated (using the SBMFA), no further approximations are needed to obtain  $\rho_n^K(\omega)$ .
- [76] In Ref. [66], the authors take the system out of the particle-hole symmetric point and multiply the integrand by a Fermi function. In order to keep our system in the particle-hole symmetric point, where it is deep into the Kondo regime, we opted for taking the absolute value  $|\rho_n^K(\omega) - \rho_n^{NK}(\omega)|$  of the integrand.
- [77] P. W. Anderson, *J. Phys. C* **3**, 2436 (1970).
- [78] We chose to denote the sites in the semi-infinite chain using the symbol “ $n$ ” [which then becomes the argument for the LDOS function  $L(n)$ ]. However, the *integrated* spin correlation in site “ $N$ ” is a sum of spin correlations from site  $n = 1$  to site  $n = N$ , i.e.,  $\Sigma(N) = \sum_{n=1}^N \langle \vec{S}_d \cdot \vec{S}_n \rangle$ , therefore, the integrated spin correlation is denoted as a function of  $N$ . In addition, for the sake of convenience, we define  $\Sigma(0) = -\langle \vec{S}_d^2 \rangle = -3/8$ , where  $\vec{S}_d$  is the spin operator for the magnetic impurity.
- [79] The comment made in Ref. [75] is also relevant for the calculation of the  $n$ -dependent quantities to be used in Eq. (8). Indeed, once the Green's function at the impurity is known, the EOM can be used to calculate the Green's function needed to calculate  $\langle c_d^\dagger c_n \rangle$  and its Hermitian conjugate, and this procedure does not require any further approximations.
- [80] T. Hand, J. Kroha, and H. Monien, *Phys. Rev. Lett.* **97**, 136604 (2006).
- [81] S. Costamagna, C. J. Gazza, M. E. Torio, and J. A. Riera, *Phys. Rev. B* **74**, 195103 (2006).
- [82] D. M. Newns and N. Read, *Adv. Phys.* **36**, 799 (1987).
- [83] J. Hubbard, *Proc. R. Soc. London, Ser. A* **276**, 238 (1963).